

Implications of PREX-2 on the electric dipole polarizability of neutron rich nuclei

J. Piekarewicz^{1,*}

¹*Department of Physics, Florida State University, Tallahassee, FL 32306, USA*

(Dated: May 31, 2021)

Background: The recent announcement by the PREX collaboration of an unanticipated thick neutron skin in ^{208}Pb (R_{skin}^{208}) has challenged our understanding of neutron rich matter in the vicinity of nuclear saturation density. Whereas earlier constraints indicate that the symmetry energy is relatively soft, the PREX-2 result seems to suggest the opposite.

Purpose: To confront constraints on the symmetry energy obtained from measurements of the electric dipole polarizability against those informed by the PREX-2 measurement of R_{skin}^{208} and by the correlations that it entails.

Methods: Covariant energy density functionals informed by the properties of finite nuclei are used to compute the electric dipole response of ^{48}Ca , ^{68}Ni , ^{132}Sn , and ^{208}Pb . The set of functionals used in this work are consistent with experimental data, yet are flexible enough in that they span a wide range of values of R_{skin}^{208} .

Results: It is found that theoretical predictions of the electric dipole polarizability that are consistent with the PREX-2 measurement systematically overestimate the corresponding values extracted from the direct measurements of the distribution of electric dipole strength.

Conclusions: The neutron skin thickness of ^{208}Pb extracted from parity violating electron scattering and the electric dipole polarizability measured in photoabsorption experiments are two of the cleanest experimental tools used to constrain the symmetry energy around nuclear saturation density. However, the recent value of R_{skin}^{208} that suggests a fairly stiff symmetry energy stands in stark contrast to the conclusions derived from the electric dipole polarizability. At present, we offer no solution to this dilemma.

PACS numbers: 21.60.Jz, 24.10.Jv, 24.30.Cz, 26.60.Kp,

I. INTRODUCTION

Experiments with electroweak probes provide an effective strategy to elucidate the complex nuclear dynamics. This stands in contrast to experiments involving hadronic probes that are often plagued by considerable model dependencies and uncontrolled approximations [1]. Beside their intrinsic value in the determination of fundamental nuclear properties, electroweak experiments provide a clean and powerful link to the equation of state (EOS) of neutron rich matter. Indeed, laboratory experiments provide the first rung in a “density ladder” that aims to determine the EOS over a wide range of densities.

The quest to determine the EOS has been reenergized by the plethora of recent astronomical discoveries that include the identification of massive neutron stars [2–5], the simultaneous determination of the mass and radius of two neutron stars [6–10], and the detection of gravitational waves from a binary neutron star merger [11]. These historic discoveries have placed stringent constraints on the EOS at densities above two-to-three times nuclear saturation density.

Among the electroweak experiments that have been identified as having a strong impact on the EOS of neutron-rich matter (i.e., strong isovector indicators) are parity-violating electron scattering [12–14] and photoabsorption reaction [15–22]. For such class of experiments,

the connection to the equation of state emerges from a correlation between the slope of the symmetry energy at saturation density (L) and both the neutron skin thickness of ^{208}Pb (R_{skin}^{208}) [23–26] and the product of the electric dipole polarizability α_D times the value of the nuclear symmetry energy at saturation density J [27–29].

Given the importance of the symmetry energy in constraining a host of neutron-star properties—particularly stellar radii [30]—a concerted community effort has been devoted to determine the symmetry energy and its slope at saturation density. For example, from one of the latest compilations [31], the recommended values for these two parameters are

$$J = (31.7 \pm 1.1) \text{ MeV}, \quad (1a)$$

$$L = (59.8 \pm 4.1) \text{ MeV}. \quad (1b)$$

The above values are in good agreement with other estimates that were obtained from either purely theoretical approaches or extracted from a theoretical interpretation of experimental data [29, 31–38]; see Fig. 2 of Ref. [31]. Based on such a preponderance of evidence, it was concluded that the symmetry energy in the vicinity of nuclear saturation density is relatively soft. That is, the pressure increases slowly with increasing density.

However, all this evidence was collected prior to the completion of the latest Lead Radius EXperiment (PREX-2) at Jefferson Lab [14]. Due to problems during the first phase of the experiment (“PREX-1”) the reported error bars at that time were simply too large

* jpiekarewicz@fsu.edu

to place any meaningful constraint on the equation of state. Indeed, the first report from the PREX collaboration [12]—together with the strong linear correlation between R_{skin}^{208} and L identified in Ref. [26]—yielded the following results:

$$R_{\text{skin}}^{208} = \left(0.33^{+0.16}_{-0.18}\right) \text{ fm}, \quad (2a)$$

$$35 \lesssim L(\text{MeV}) \lesssim 265. \quad (2b)$$

The PREX-2 campaign has dramatically changed the landscape by delivering on the original promise to determine the neutron radius of ^{208}Pb with a ~ 0.06 fm (or 1%) precision. By combining the PREX-1 and PREX-2 measurements, the improved value of R_{skin}^{208} was reported to be [14]

$$R_{\text{skin}} = (0.283 \pm 0.071) \text{ fm}. \quad (3)$$

Using this newly reported value—together with the strong correlation between R_{skin}^{208} and both the symmetry energy J and its slope L at saturation density—the following 1σ intervals were obtained [39]:

$$J = (38.1 \pm 4.7) \text{ MeV}, \quad (4a)$$

$$L = (106 \pm 37) \text{ MeV}. \quad (4b)$$

These updated results greatly overestimate the central value and uncertainty quoted in Eq.(1). Given that some

of the earlier limits on both J and L were inferred from the analysis of the electric dipole polarizability of a few neutron-rich nuclei, it is the aim of this paper to confront those earlier results against the new limits obtained from incorporating the PREX-2 recommended value for R_{skin}^{208} .

The manuscript has been organized as follows. In Sec.II we review some of the most salient features of the theoretical framework used to compute the electric dipole response. Predictions, informed by the recent PREX-2 measurement, are made in Sec.III for the electric dipole polarizability of ^{48}Ca , ^{68}Ni , ^{132}Sn , and ^{208}Pb . These predictions are later compared against the experimentally recommended values obtained from photoabsorption experiments. Finally, we present a short summary and conclusions in Sec.IV.

II. FORMALISM

The theoretical framework implemented in this work has been presented in much greater detail in several references, so we limit ourselves to highlight the most relevant points; see for example [40, 41] and references contained therein. The starting point for the relativistic calculation of the nuclear response is the covariant model of Ref. [42] supplemented by an isoscalar-isovector term originally introduced in Ref. [43]. That is, the interacting Lagrangian density is given by

$$\begin{aligned} \mathcal{L}_{\text{int}} = & \bar{\psi} \left[g_s \phi - \left(g_v V_\mu + \frac{g_\rho}{2} \boldsymbol{\tau} \cdot \mathbf{b}_\mu + \frac{e}{2} (1 + \tau_3) A_\mu \right) \gamma^\mu \right] \psi \\ & - \frac{\kappa}{3!} (g_s \phi)^3 - \frac{\lambda}{4!} (g_s \phi)^4 + \frac{\zeta}{4!} g_v^4 (V_\mu V^\mu)^2 + \Lambda_v \left(g_\rho^2 \mathbf{b}_\mu \cdot \mathbf{b}^\mu \right) \left(g_v^2 V_\nu V^\nu \right). \end{aligned} \quad (5)$$

The Lagrangian density includes as the basic degrees of freedom an isodoublet nucleon field ψ interacting through the exchange of photons (A_μ) and three massive “mesons”: a scalar-isoscalar (ϕ) a vector-isoscalar (V^μ), and a vector-isovector (\mathbf{b}_μ) [44–46]. The isoscalar-isovector coupling constant Λ_v is highly sensitive to the density dependence of symmetry energy—and in particular to its slope at saturation density L [43]. Useful to the calibration of the model is the existence of an analytic—one-to-one—correspondence between bulk parameters of infinite nuclear matter and the various coupling constants. In particular, there is a one-to-one correspondence between the two isovector parameters (g_ρ and Λ_v) and the value of symmetry energy J and its slope L at saturation density [47].

Once the calibration of the functional is completed, one proceeds to compute ground-state properties of finite nuclei by solving self-consistently the resulting Kohn-Sham equations [41]. Among the ground state properties that emerge is a set of single-particle energies, a corresponding set of Dirac orbitals, the Kohn-Sham potentials, and

neutron and proton densities. In turn, the dynamic response of the system to an external probe is computed in a relativistic random phase approximation (RPA). The consistent nuclear response of the ground state is encoded in the RPA formalism that ensures that important symmetries are maintained [40]. Indeed, by employing a residual particle-hole interaction consistent with the interaction used to generate the mean-field ground state, the conservation of the vector current is preserved and the spurious strength associated with a uniform translation of the center of mass is decoupled from the physical response [40].

The cornerstone of the theoretical framework is the polarization tensor, whose imaginary part is directly connected to the experimentally accessible nuclear response [48, 49]. In particular, the distribution of electric dipole ($E1$) strength of interest in this work can be isolated from the longitudinal response that is defined as

follows:

$$S_L(q, \omega) = \sum_n \left| \langle \Psi_n | \hat{\rho}(\mathbf{q}) | \Psi_0 \rangle \right|^2 \delta(\omega - \omega_n). \quad (6)$$

Here Ψ_0 is the exact nuclear ground state, Ψ_n is an excited state with excitation energy $\omega_n = E_n - E_0$, and $\hat{\rho}(\mathbf{q})$ is the transition operator that is given as the Fourier transform of the vector-isovector density. That is,

$$\hat{\rho}_a(\mathbf{q}) = \int d^3r \bar{\psi}(\mathbf{r}) e^{-i\mathbf{q}\cdot\mathbf{r}} \gamma^0 \tau_3 \psi(\mathbf{r}), \quad (7)$$

where $\gamma^0 = \text{diag}(1, 1, -1, -1)$ is the zeroth component of the Dirac matrices and $\tau_3 = \text{diag}(1, -1)$ is the third component of the Pauli matrices in isospin space.

To lowest order, the uncorrelated polarization describes particle-hole excitations between the single-particle orbitals obtained from solving the Kohn-Sham equations. The RPA response goes beyond the uncorrelated response by building collectivity through the mixing of all particle-hole excitations with the same quantum numbers. If many particle-hole pairs close in energy are involved and the residual particle-hole interaction is strong, then the nuclear response is strongly collective and one ‘‘giant resonance’’ dominates. In the non-spectral framework employed in this work, the continuum width of the resonance—obtained from exciting a bound nucleon into the continuum—is treated exactly. Not so, however, the spreading width, which is driven by more complex configurations. This is a well-known deficiency of the RPA approach.

In the long wavelength limit, the distribution of isovector dipole strength $R(\omega; E1)$ is related to the longitudinal response through the following equation:

$$R(\omega; E1) = \lim_{q \rightarrow 0} \left(\frac{9}{4\pi q^2} \right) S_L(q, \omega; E1), \quad (8)$$

which in turn, is directly related to the photoabsorption cross section

$$\sigma_{\text{abs}}(\omega) = \frac{16\pi^3}{9} \frac{e^2}{\hbar c} \omega R(\omega; E1). \quad (9)$$

Widely used in the literature are the following moments of the distribution of strength: (a) the energy weighted sum m_1 ; (b) the energy unweighted sum m_0 , and (c) the inverse energy weighted sum m_{-1} , which is proportional to the electric dipole polarizability [see Eq.(11)]. Centroid energies of collective resonances are defined as $E_c = m_1/m_0$, with the m_1 moment ‘‘protected’’ by the (largely) model-independent energy weighted sum rule (EWSR) [50]:

$$m_1 = \frac{9\hbar^2}{8\pi M} \left(\frac{NZ}{A} \right) \approx 14.8 \left(\frac{NZ}{A} \right) \text{fm}^2 \text{MeV}. \quad (10)$$

Being model independent, the EWSR is not effective at discriminating among various theoretical models. Instead, the electric dipole polarizability has been identified

as a strong isovector indicator [51] that is highly sensitive to the stiffness of the symmetry energy [52]. The electric dipole polarizability is defined as follows:

$$\alpha_D = \frac{\hbar c}{2\pi^2} \int_0^\infty \frac{\sigma_{\text{abs}}(\omega)}{\omega^2} d\omega = \frac{8\pi e^2}{9} m_{-1}. \quad (11)$$

It is the powerful connection between the photoabsorption cross section $\sigma_{\text{abs}}(\omega)$, α_D , and L that we will examine in the next section.

III. RESULTS

In this section we present results for the electric dipole response of four neutron-rich nuclei: ^{48}Ca , ^{68}Ni , ^{132}Sn , and ^{208}Pb . Given that our main goal is to constrain bulk properties of the symmetry energy, these four spherical nuclei were chosen to minimize uncertainties associated with certain nuclear-structure effects, such as pairing correlations. Moreover, with the exception of ^{132}Sn , data already exists for the electric dipole polarizability of ^{208}Pb [15], ^{68}Ni [17, 18], and ^{48}Ca [20].

To assess the impact on the electric dipole polarizability from the combined PREX-1–PREX-2 measurements (henceforth referred simply as ‘‘PREX-2’’) we make predictions for the distribution of electric dipole strength using a set of covariant energy density functionals (EDFs) that span a wide range of values for the neutron skin thickness of ^{208}Pb . These functionals include FSUGold2 [47], together with a set of six systematically varied interactions—FSUGold2–L047, L054, L058, L076, L090, L100—that have identical isoscalar properties as FSUGold2, but isovector properties defined by a preselected value for the slope of the symmetry energy [39]. For example, FSUGold2–L100 was calibrated with an input value of $L = 100$ MeV. Another set of accurately calibrated density functionals is given by RMF016, RMF022, RMF032 [53], where now the labels are associated to the predicted value of R_{skin}^{208} . For example, RMF032 predicts a neutron skin thickness of $R_{\text{skin}}^{208} = 0.32$ fm. Finally, TFA, TFB, and TFC, with $R_{\text{skin}}^{208} = 0.25, 0.30,$ and 0.33 fm, respectively, were calibrated to test whether the large central value of $R_{\text{skin}}^{208} = 0.33$ fm originally reported by the PREX collaboration [12] was incompatible with other laboratory experiments and/or astrophysical observations [54]. Now as then, we find no compelling reason to rule out models with large neutron skins. Additional details on the fitting protocol—including a description of the model and the observables used in the calibration procedure—may be found in Refs. [47, 53, 54].

The models considered here span a wide range of values for both the neutron skin thickness of ^{208}Pb and the associated slope of the symmetry energy L . Such a range is comparable to the one used in the multi-model analysis of the sensitivity of the symmetry energy to the electric dipole polarizability and weak-charge form factor of both ^{48}Ca and ^{208}Pb [52, 55]. Nevertheless, given that the present study relies on a specific class of covariant EDFs,

all the results presented here should be tested against other theoretical approaches.

A. Neutron Skins: Data-to-Data Relations

Although the primary goal of this work is to confront constraints on the density dependence of the symmetry energy extracted from measurements of the electric dipole polarizability against those derived from PREX-2, we start by displaying in Fig.1 predictions for the neutron skin thickness of ^{48}Ca , ^{68}Ni , and ^{132}Sn inferred from the PREX-2 measurement. The numbers associated with each straight line represent the correlation coefficient (nearly one in all three cases) and the shaded region indicates the 1σ PREX-2 error in R_{skin}^{208} [14]. Relying on the nearly perfect correlations displayed in the figure, the following “data-to-data” relations are inferred for the neutron skin thickness of these three neutron rich nuclei:

$$R_{\text{skin}}^{48} = (0.229 \pm 0.035) \text{ fm}, \quad (12a)$$

$$R_{\text{skin}}^{68} = (0.267 \pm 0.050) \text{ fm}, \quad (12b)$$

$$R_{\text{skin}}^{132} = (0.350 \pm 0.074) \text{ fm}. \quad (12c)$$

The prediction for ^{48}Ca is particularly timely given that

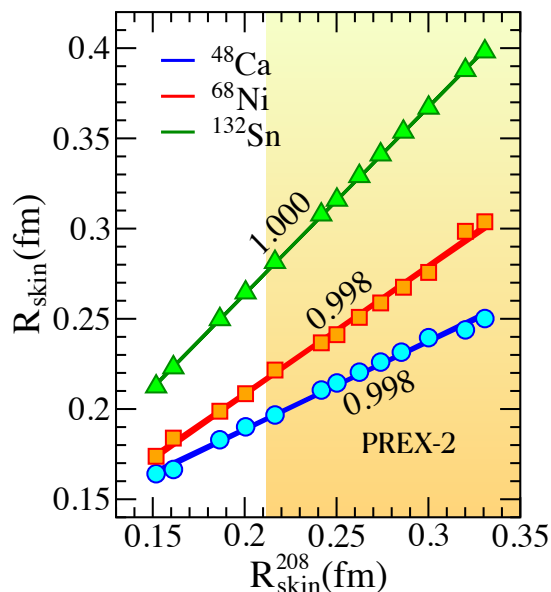


FIG. 1. (Color online). Emergence of a *data-to-data* relation between the neutron skin thickness of ^{208}Pb and the corresponding neutron skin thickness of ^{48}Ca , ^{68}Ni , and ^{132}Sn . The numbers above the lines indicate the value of the correlation coefficients and the shaded area denotes the 1σ interval reported by PREX-2 [14].

the *Calcium Radius EXperiment* (CREX) has been completed and the analysis is currently under way. CREX measured the weak-charge form factor of ^{48}Ca with a high-enough precision to allow for the extraction of the

neutron radius with an anticipated experimental error of $\sim 0.03 \text{ fm}$ [56], that is similar to the one quoted in Eq.(12a).

Part of the appeal of ^{48}Ca —and a main motivation behind the experiment [56]—is that it provides a powerful bridge between microscopic approaches and density functional theory. In the particular case of ab-initio approaches rooted in coupled cluster theory, the prediction of $0.12 \text{ fm} \lesssim R_{\text{skin}}^{48} \lesssim 0.15 \text{ fm}$ [38], lies well outside the 1σ region quoted in Eq.(12a). On the other hand, a combined theoretical-experimental approach based on a dispersion-optical model predicts a best-fit value that is significantly larger: $R_{\text{skin}}^{48} = (0.249 \pm 0.023) \text{ fm}$ [57], a value that was later revised to $R_{\text{skin}}^{48} = (0.22 \pm 0.03) \text{ fm}$ [58]. The revised value is in excellent agreement with the PREX-2 informed value quoted in Eq.(12a).

We note that the determination of the neutron skin thickness of a variety of neutron-rich nuclei is one of the main science drivers of the Facility for Rare Isotope Beams (FRIB) [59]. Given that many of these experiments will involve unstable nuclei in inverse kinematics, CREX and PREX-2 will provide critical anchors for the calibration of hadronic reactions.

B. Correlating R_{skin}^{208} to $J\alpha_D$

The electric dipole polarizability was identified by Reinhard and Nazarewicz as a strong isovector indicator that is highly sensitive to the density dependence of the symmetry energy [51]. Whereas the correlation between the electric dipole polarizability and the neutron skin thickness is strong, a far stronger correlation exists between R_{skin}^{208} (or L) and the product of J times the electric dipole polarizability [27, 28]. Indeed, Fig. 2 displays the nearly perfect correlation between R_{skin}^{208} and $J\alpha_D$ for all four nuclei considered in this work. As in Fig.1, the numbers next to the lines display the correlation coefficients and the shaded region indicates the PREX-2 error [14]. Relying on the nearly perfect correlation between R_{skin}^{208} and $J\alpha_D$, we can extract the following 1σ intervals for all four nuclei of interest:

$$J\alpha_D^{48} = (88.4 \pm 15.4) \text{ MeV fm}^3, \quad (13a)$$

$$J\alpha_D^{68} = (174 \pm 33.0) \text{ MeV fm}^3, \quad (13b)$$

$$J\alpha_D^{132} = (422 \pm 84.6) \text{ MeV fm}^3, \quad (13c)$$

$$J\alpha_D^{208} = (830 \pm 150) \text{ MeV fm}^3. \quad (13d)$$

These numbers will become important for the statistical analysis that will be carried out in the following sections.

C. Electric Dipole Response of ^{208}Pb

In this section we explore the impact of PREX-2 on the electric dipole polarizability of ^{208}Pb . A high-precision measurement of the electric dipole response of

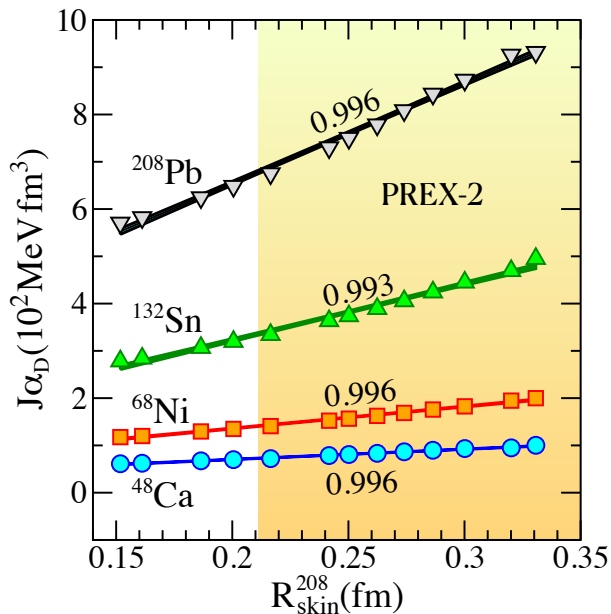


FIG. 2. (Color online). Correlation between the neutron skin thickness of ^{208}Pb and the product of the nuclear symmetry energy at saturation density times the electric dipole polarizability of ^{48}Ca , ^{68}Ni , ^{132}Sn , and ^{208}Pb . The numbers above the lines indicate the value of the correlation coefficients and the shaded area denotes the 1σ error reported by PREX-2 [14].

^{208}Pb was obtained from the small-angle (\mathbf{p}, \mathbf{p}') scattering experiment carried out at the RCNP facility in Osaka, Japan [15]. Using two independent techniques—plus a careful comparison against existing photoabsorption data—the following value for the electric dipole polarizability was obtained: $\alpha_D^{208} = (20.1 \pm 0.6) \text{ fm}^3$. The precision attained by the RCNP experiment, together with the strong correlation between the neutron skin thickness and the electric dipole polarizability identified in Ref. [60], resulted in the following recommended value for the neutron skin thickness of ^{208}Pb [15]:

$$R_{\text{skin}}^{208} = 0.156_{-0.021}^{+0.025} \text{ fm}. \quad (14)$$

Following the same approach described in Ref. [60]—but now using a large and diverse set of EDFs—a slightly revised value was obtained: $0.13 \leq R_{\text{skin}}^{208} \leq 0.19 \text{ fm}$ [29], confirming the initial estimate deduced from the RCNP experiment. These values, however, stand in stark contrast to the much larger value reported by the PREX collaboration [14].

To elucidate the source of this discrepancy, we start by displaying in Fig. 3(a) the distribution of electric dipole strength weighted by the inverse of the excitation energy: $m_{-1}(\omega) \equiv R(\omega; E1)/\omega$. The set of 13 covariant EDFs are all consistent with ground state properties of finite nuclei, yet they are flexible enough in that they span a wide range of values of R_{skin}^{208} , as indicated by the labels in the figure. Unlike the EWSR that is largely model independent [50], the inverse energy weighted sum displays a significant model dependence. Indeed, models with a stiff

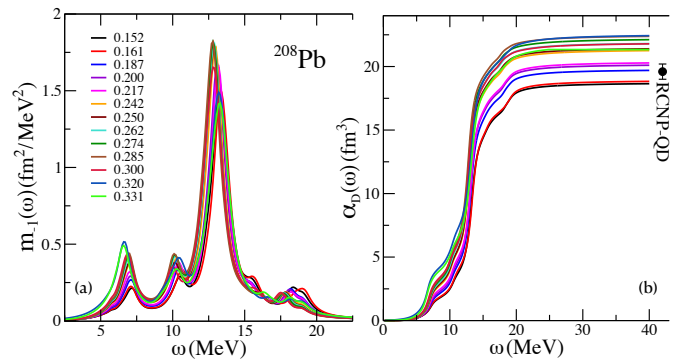


FIG. 3. (Color online). (a) Inverse energy weighted dipole response of ^{208}Pb computed with a diverse set of energy density functionals that span a wide range of value for the neutron skin thickness of ^{208}Pb , as displayed by the labels in the figure. (b) Running (or cumulative) sum of the electric dipole polarizability, with the electric dipole polarizability defined as $\alpha_D \equiv \alpha_D(\omega_{\text{max}})$.

symmetry energy generate larger values for both m_{-1} and α_D [61]. This fact is illustrated in Fig. 3(b) that displays the “running (or cumulative) sum” $\alpha_D(\omega)$. The predicted value for electric dipole polarizability is given by $\alpha_D \equiv \alpha_D(\omega_{\text{max}})$, with $\omega_{\text{max}} = 40 \text{ MeV}$. Also included in Fig. 3(b) is the slightly refined value extracted from the RCNP experiment. The experimental distribution of strength contains a small, non-resonant “contaminant”—the so-called quasi-deuteron (QD) contribution—at high energies that is not accounted for in the theoretical (RPA) predictions. Hence, for a meaningful comparison against experiment, the relatively small (2.5%) quasi-deuteron contribution was removed, leading to a revised estimate of [29]

$$\alpha_D^{208} = (19.6 \pm 0.6) \text{ fm}^3. \quad (15)$$

This is the experimental value displayed in Fig. 3(b).

To properly quantify the discrepancy in the value of α_D^{208} extracted from the RCNP measurement relative to the one informed by PREX-2, we display in Fig. 4 the associated probability distribution functions. For the RCNP experiment, we assume a normal (or Gaussian) probability distribution with the mean and standard deviation given in Eq.(15). Instead, for the PREX-2-informed result one obtains a “normal ratio distribution”—similar in shape to the well-known skew-normal distribution. Following the derivation provided in the Appendix, one obtains the following PREX-2-informed estimate:

$$\alpha_D^{208} = (21.8_{-1.4}^{+1.1}) \text{ fm}^3, \quad (16)$$

where $\alpha_D^{208} = 21.8 \text{ fm}^3$ is the median of the distribution, and the lower and upper limits contain approximately 16% and 84% of the area under the curve. The figure illustrates the tension that emerges in comparing the two probability distributions. Indeed, the overlap region in

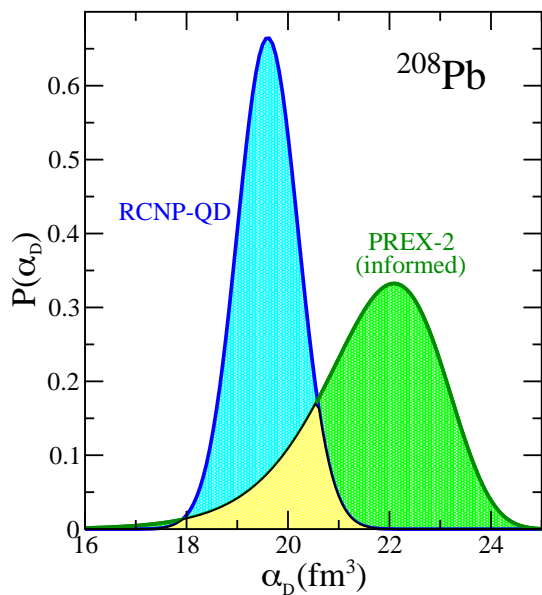


FIG. 4. (Color online). The normal probability distribution as reported by the RCNP experiment [15]—minus the quasi-deuteron (QD) contribution [29]—is compared against the normal ratio distribution informed by the PREX-2 measurement [14]. The region shaded in yellow represents the area under the curve common to both probability distributions and amounts to less than 0.25 out of a possible maximum of 1.

Fig. 4, estimated as the area under the curve shared by the two probability distributions, amounts to 0.25 out of a possible maximum of 1. An alternative definition of the variation distance between two probability distributions is given in terms of the the largest possible difference at a given point. For Fig. 4, the largest possible difference is obtained at the peak of the RCNP-QD distribution, which results in a variation distance of 0.6. A perfect overlap between the two probability distribution would be equal to zero. In isolation, Fig. 4 may not be too much of a concern. However, it is the systematic discrepancy across various nuclei that we identify as the source of the tension.

D. Electric Dipole Response of ^{48}Ca

As already mentioned, ^{48}Ca provides a powerful bridge between microscopic approaches and density functional theory. At the beginning of the section we established that coupled-cluster predictions for the neutron skin of ^{48}Ca underestimate the limits informed by PREX-2. In this section we confront both sets of predictions, but now for the electric dipole polarizability [38]. Following the same approach as in the case of ^{208}Pb , the distribution of inverse-energy-weighted strength $m_{-1}(\omega)$ is displayed in Fig. 5, alongside the running sum and the experimental value of α_D^{48} reported by Birkhan and collaborators [20]. The labels in the figure continue to identify the various

models by the predictions for R_{skin}^{208} (not R_{skin}^{48}). The inset in the figure confirms that the experimental value of α_D^{48} favors models with a relatively soft symmetry energy, although the case is not as convincing as for ^{208}Pb because of the fairly large error bar. The impact of the large error bar can be better appreciated in Fig. 6 where the overlap region between the two probability distributions has now increased to about 0.5. Experimental values for α_D^{48} can

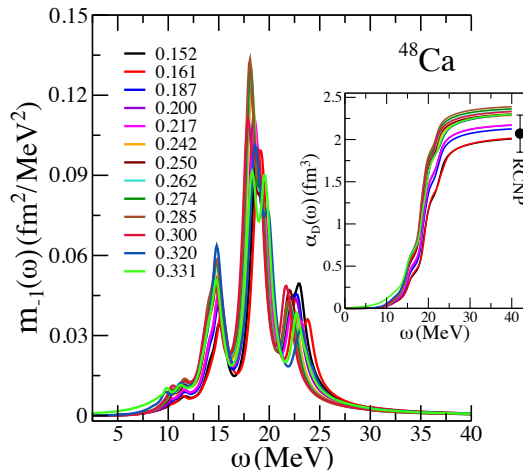


FIG. 5. (Color online). Inverse energy weighted dipole response of ^{48}Ca computed with a diverse set of energy density functionals that span a wide range of value for the neutron skin thickness of ^{208}Pb , as displayed by the labels in the figure. The inset displays the running (or cumulative) sum of the electric dipole polarizability, with the electric dipole polarizability defined as $\alpha_D \equiv \alpha_D(\omega_{\text{max}})$.

now be collected from the RCNP experiment [20], the ab-initio/coupled-cluster predictions of Hagen and collaborators [38], and from the one obtained here by invoking the PREX-2 measurement. One obtains,

$$\alpha_D^{48}(\text{fm}^3) = \begin{cases} 2.07 \pm 0.22, & \text{RCNP [20]} \\ 2.39 \pm 0.21, & \text{ab-initio [38]} \\ 2.32^{+0.10}_{-0.13}, & \text{this work.} \end{cases} \quad (17)$$

Although there is a noticeable difference in the central values between theory and experiment, the error bars are simply too large to draw any firm conclusion. This is an area in which the proposed, high-intensity Gamma Factory at CERN could be of enormous value [62–64].

It is important to note that whereas the prediction from the ab-initio formalism for α_D^{48} is fully consistent with the one suggested in this work, the corresponding predictions for R_{skin}^{48} differ significantly, further suggesting that the strong isovector indicator is $J\alpha_D^{48}$ and not α_D^{48} alone. Indeed, the extracted value of $J \approx 38$ MeV from the PREX-2 measurement is considerably larger than the $J \lesssim 30$ MeV prediction from ab-initio calculations [38].

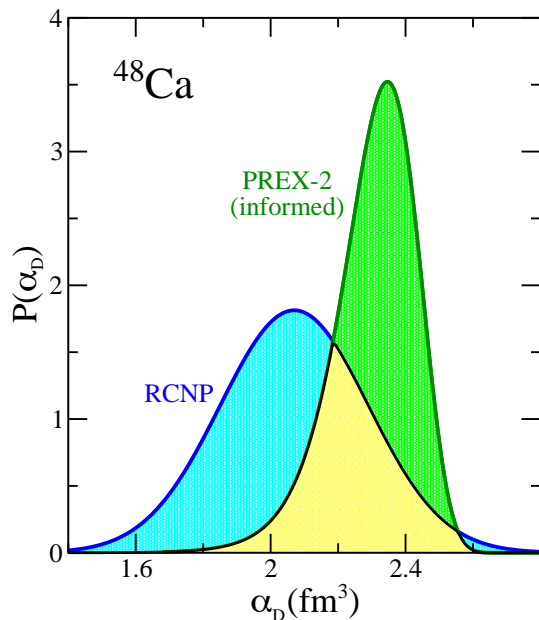


FIG. 6. (Color online). The normal probability distribution as reported by the RCNP experiment [20] is compared against the normal ratio distribution informed by the PREX-2 measurement [14]. The region shaded in yellow represents the area under the curve common to both probability distributions and amounts to about 0.5 out of a possible maximum of 1.

E. Electric Dipole Response of ^{68}Ni

The previous two sections were devoted to address the impact of the new PREX-2 measurement on the electric dipole response of ^{208}Pb and ^{48}Ca —the only two stable, neutron-rich, doubly-magic nuclei in the entire nuclear chart. These two nuclei provide valuable anchors for the calibration and interpretation of experiments on exotic nuclei with large neutron skins at future radioactive beam facilities [1]. Given the enormous challenges involved in the commissioning and implementation of parity-violating experiments, photoabsorption reactions on exotic nuclei remain the only electroweak alternative to probe the density dependence of the symmetry energy.

The electric dipole response of the unstable, neutron-rich nucleus ^{68}Ni has been measured using Coulomb excitation in inverse kinematics at the GSI facility in Germany [17, 18]. The electric dipole polarizability of ^{68}Ni was reported to be [18]:

$$\alpha_D^{68} = (3.40 \pm 0.23) \text{ fm}^3 \xrightarrow{\text{“Tails”}} (3.88 \pm 0.31) \text{ fm}^3. \quad (18)$$

The first number represents the experimental value obtained from integrating the photoabsorption cross section between 7.8 and 28.4 MeV. In turn, the second number accounts for the extrapolations to low- and high-energy that are required for a meaningful comparison between experiment and theory [29]. This second, slightly larger, value is denoted by “GSI+Tails” on the inset of Fig. 7.

An interesting feature displayed in Fig. 7 is the significant amount of low-energy (“Pygmy”) strength that is identified below the giant resonance region. Although the interpretation of its character is still under debate [65–69], the pygmy dipole resonance is often portrayed as an oscillation of the excess neutrons against the isospin symmetric core. Besides its interest as an exotic mode of excitation, the emergence of low-energy dipole strength has been found to correlate strongly with the development of a neutron rich skin [70]. This finding provides a compelling connection between the electric dipole polarizability and the neutron skin thickness—two critical observables used in the determination of the slope of the symmetry energy. Based on the results displayed in the inset of Fig. 7, the electric dipole response of ^{68}Ni continues to suggest a fairly soft symmetry energy.

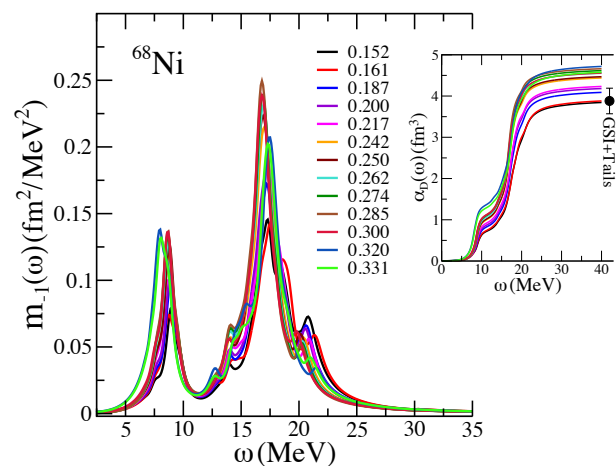


FIG. 7. (Color online). Inverse energy weighted dipole response of ^{68}Ni computed with a diverse set of energy density functionals that span a wide range of value for the neutron skin thickness of ^{208}Pb , as displayed by the labels in the figure. The inset displays the running (or cumulative) sum of the electric dipole polarizability, with the electric dipole polarizability defined as $\alpha_D \equiv \alpha_D(\omega_{\text{max}})$.

And not surprisingly, a tension develops between the results extracted directly from the GSI experiment and those constrained by PREX-2. In the case of the GSI experiment, the following value for the neutron skin thickness of ^{68}Ni was reported [18]:

$$R_{\text{skin}}^{68} = (0.17 \pm 0.02) \text{ fm}, \quad (19)$$

a value that is notably below the PREX-2-informed value of $R_{\text{skin}}^{68} \approx 0.27 \text{ fm}$ quoted in Eq. (12b). We conclude this subsection by displaying in Fig. 8 the experimental probability distribution alongside the normal ratio distribution inferred from PREX-2. Consistent with earlier findings, the latter is shifted to higher values relative to the former, with an overlap region that amounts to only 28%.

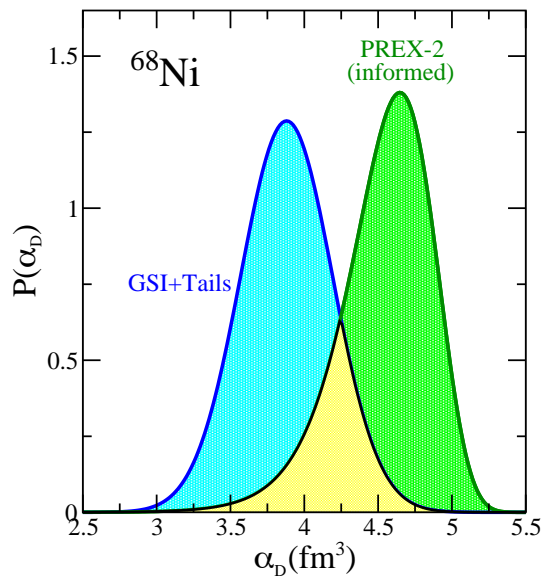


FIG. 8. (Color online). The normal probability distribution as reported by the GSI experiment [18]—plus the addition of low- and high-energy tails [29]—is compared against the normal ratio distribution informed by the PREX-2 measurement [14]. The region shaded in yellow represents the area under the curve common to both probability distributions and amounts to less than 0.3 out of a possible maximum of 1.

That is,

$$\alpha_D^{68}(\text{fm}^3) = \begin{cases} 3.88 \pm 0.31, & \text{GSI+Tails [18, 29]} \\ 4.58_{-0.33}^{+0.26}, & \text{this work.} \end{cases} \quad (20)$$

F. Electric Dipole Response of ^{132}Sn

Lastly, predictions are displayed in Fig. 9 for the unstable, doubly-magic, neutron-rich nucleus ^{132}Sn . Although a measurement of the electric dipole response of ^{132}Sn —both in the low- (Pygmy) and high-energy (Giant) regions—has been reported in Ref. [71], a precise value of the electric dipole polarizability is not yet available. Nevertheless, given that several experimental campaigns are being planned to measure the electric dipole response of ^{132}Sn , it is pertinent to provide some predictions. Based on the dipole response of ^{68}Ni , one would expect the emergence of a significant amount of low-energy strength. In fact, it was shown in Ref. [70] how the emergence of low-energy dipole strength correlates with the development of a neutron-rich skin along the tin isotopes, from ^{100}Sn all the way to ^{132}Sn . However, it was also observed that as the $h_{11/2}$ neutron orbital was progressively filled, the low-energy strength “saturates” at ^{120}Sn , indicating that high-angular momentum orbitals play a minor role in driving low-energy transitions of low multipolarity (see Figs. 4-5 of Ref. [70]). One of the main virtues of ^{132}Sn relative to the lighter open-shell isotopes

lies in its simple structure since, as a doubly-magic nucleus, ^{132}Sn is insensitive to the (presently unclear) role of pairing correlations [22].

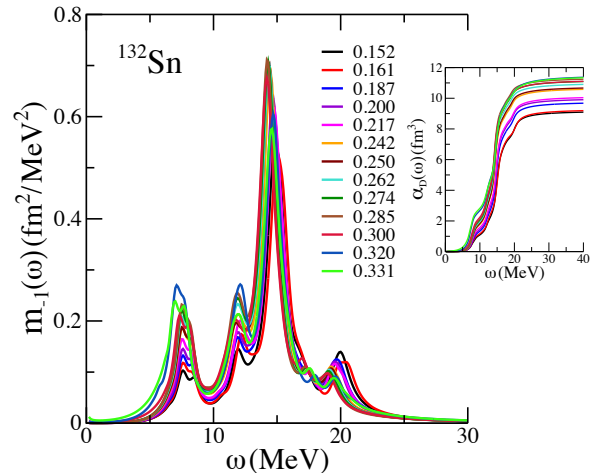


FIG. 9. (Color online). Inverse energy weighted dipole response of ^{132}Sn computed with a diverse set of energy density functionals that span a wide range of value for the neutron skin thickness of ^{208}Pb , as displayed by the labels in the figure. The inset displays the running (or cumulative) sum of the electric dipole polarizability, with the electric dipole polarizability defined as $\alpha_D \equiv \alpha_D(\omega_{\text{max}})$.

A precise measurement of the electric dipole polarizability of ^{132}Sn is well motivated given the two model independent correlations connecting ^{132}Sn to ^{208}Pb identified in Ref. [52], one for the neutron skin thickness and the other one for the electric dipole polarizability. This would suggest that a measurement of R_{skin}^{132} (if feasible) should mirror the PREX-2 result and yield a correspondingly large value for the neutron skin thickness of ^{132}Sn , confirming that the symmetry energy is stiff. On the other hand, if one follows the α_D correlation, then the relatively low value of α_D^{208} reported by the RCNP experiment would also imply a low value for electric dipole polarizability of ^{132}Sn , suggesting instead that the symmetry energy is soft.

The above situation can be precisely quantified. For example, invoking the RCNP measurement of α_D^{208} , one would infer on the basis of the strong correlations uncovered in Ref. [52] the following values for ^{132}Sn :

$$R_{\text{skin}}^{132} = (0.23 \pm 0.02) \text{ fm}, \quad (21a)$$

$$\alpha_D^{132} = (10.08 \pm 0.15) \text{ fm}^3. \quad (21b)$$

In contrast, if one relies on the recent PREX-2 analysis, then one infers a normal ratio distribution from which the significantly larger values are obtained:

$$R_{\text{skin}}^{132} = (0.35 \pm 0.07) \text{ fm}, \quad (22a)$$

$$\alpha_D^{132} = (11.07_{-0.97}^{+0.75}) \text{ fm}^3. \quad (22b)$$

IV. CONCLUSIONS

Borrowing a term from cosmology, the density ladder is a succession of theoretical, experimental, and observational techniques aimed to determine the equation of state of neutron star matter at increasingly higher densities. Laboratory experiments sensitive to the dynamics of neutron rich matter in the vicinity of nuclear saturation density provide the first rung of such a ladder. In this context, electroweak probes provide the cleanest connection to the equation of state.

Earlier estimates of the symmetry energy based on measurements of the electric dipole polarizability suggest that the symmetry energy is relatively soft. The softness of the symmetry energy was later validated by theoretical approaches as well as a large suite of experiments [31, 34]. However, the suggestion of a soft symmetry energy has now been brought into question by the recent report of an unexpectedly large neutron skin thickness in ^{208}Pb [14]. By exploiting the strong correlation between R_{skin}^{208} and L , it has been suggested that the symmetry energy is, instead, fairly stiff [39]. Connecting PREX-2 to various neutron star properties was recently explored in Refs. [39, 72].

In this paper we assessed the impact of PREX-2 on the electric dipole polarizability of several closed-shell nuclei and compared our results against those values extracted directly from experiment. A set of covariant energy density functionals that span a wide range of values of R_{skin}^{208} was used to compute ground state densities and the electric dipole response of ^{208}Pb , ^{48}Ca , ^{68}Ni , and ^{132}Sn . Relying on the nearly perfect correlation between R_{skin} and both $J\alpha_{\text{D}}$ [28] and J [39] for the class of models explored in this work, we derived limits on α_{D} informed by PREX-2. In all instances, the electric dipole polarizability informed by PREX-2 overestimated the corresponding values obtained directly from earlier measurements of the dipole response. So while direct measurements of the electric dipole polarizability seem to suggest that the symmetry energy is soft at nuclear densities, the PREX-2-informed values suggest the opposite. Given the vital role that terrestrial experiments play in constraining the slope of the symmetry energy L , the resolution of this dilemma is of utmost importance.

Naturally, one would like to see a significant reduction in the experimental uncertainty. However, prospects of a more precise electroweak determination of R_{skin}^{208} are slim, given that the PREX campaign is now over. A factor of two improvement may be possible at the Mainz Energy-recovery Superconducting Accelerator (MESA), but the timing is not optimal as the facility is currently under construction [73]. The prospects for improving the precision in the determination of α_{D} are significantly better with the commissioning of a Gamma Factory at CERN, the implementation of reactions with relativistic radioactive beams (R3B) at FAIR, and the combination of high yields and high energies for very neutron-rich isotopes that will be available at FRIB400. The challenges in

this arena are associated with the production of unstable nuclei with large skins as well as the determination of the electric dipole response over a wide range of energies. In particular, the low-energy region—above and below the neutron separation energy—is of critical importance given the significant contribution of the soft dipole (Pygmy) mode to the electric dipole polarizability. As we enter the golden age of neutron-star physics [74], a sustained and concerted community effort in both experiment and theory is both timely and important.

Appendix

The aim of this appendix is to derive the probability distribution $f(x)$ for the ratio of two normally distributed observables (x_1 and x_2) that are perfectly correlated. The resulting distribution $f(x)$ displays a “normal ratio distribution”, which in the case of Figs. 4, 6, and 8 strongly resembles the well-known skew-normal probability distribution.

The derivation of $f(x)$ hinges on the strong correlation—at least within the models employed in this work—between the neutron skin thickness of ^{208}Pb and both the symmetry energy at saturation density J [39] and the product of J times the electric dipole polarizability displayed in Fig. 2. Conceptually, computing the probability distribution is easy to understand from the perspective of statistical sampling. Assuming a Gaussian distribution for the neutron skin thickness of ^{208}Pb with a mean of $\mu = 0.283$ fm and a standard deviation of $\sigma = 0.071$ fm [14], one draws individual samples of R_{skin}^{208} using, for example, the Box–Muller transform. Then, assuming that the correlation between R_{skin}^{208} and both J and $J\alpha_{\text{D}}$ is perfect (as they nearly are!) one can in turn generate the associated values for J and $J\alpha_{\text{D}}$. Then, by simply dividing the latter over the former one obtains individual values for α_{D} that obey a normal ratio distribution as displayed in Figs. 4, 6, and 8.

However, a closed-form expression may also be derived for the normal ratio distribution. To do so, one starts with a standard Gaussian distribution of zero mean and unit standard deviation. That is,

$$f(\epsilon) = \frac{1}{\sqrt{2\pi}} e^{-\epsilon^2/2}. \quad (\text{A.1})$$

Any normal distribution $f(x)$ with a mean of μ and standard deviation of σ can be readily mapped into the above distribution by simply letting $x = \mu + \sigma\epsilon$. Let us then assume the existence of two perfectly correlated observables X_1 and X_2 normally distributed with means μ_1 and μ_2 and standard deviations σ_1 and σ_2 . For a perfect correlation between observables, one can write their ratio as follows:

$$\frac{x_2}{x_1} \equiv x = \left(\frac{\mu_2 + \sigma_2\epsilon}{\mu_1 + \sigma_1\epsilon} \right) \Rightarrow \epsilon = - \left(\frac{\mu_2 - \mu_1 x}{\sigma_2 - \sigma_1 x} \right). \quad (\text{A.2})$$

Note that the perfect correlation between X_1 and X_2 is encoded in the following relations:

$$\frac{x_2 - \mu_2}{\sigma_2} = \epsilon = \frac{x_1 - \mu_1}{\sigma_1} \Leftrightarrow \quad (\text{A.3a})$$

$$x_2 = \left(\mu_2 - \frac{\sigma_2}{\sigma_1} \mu_1 \right) + \left(\frac{\sigma_2}{\sigma_1} \right) x_1. \quad (\text{A.3b})$$

That is, the statistical sampling of $f(\epsilon)$ generates values of ϵ that determine x_1 which, in turn, determines x_2 —through the linear correlation. One can finalize the derivation of the normal ratio distribution using Eq.(A.2). That is,

$$f(\epsilon)d\epsilon = f(\epsilon(x)) \left| \frac{d\epsilon}{dx} \right| dx = f(x)dx, \quad (\text{A.4})$$

from where the normal ratio distribution is obtained:

$$f(x) = \frac{1}{\sqrt{2\pi}} \frac{|\mu_1\sigma_2 - \mu_2\sigma_1|}{(\sigma_2 - \sigma_1 x)^2} \exp \left[-\frac{1}{2} \left(\frac{\mu_2 - \mu_1 x}{\sigma_2 - \sigma_1 x} \right)^2 \right]. \quad (\text{A.5})$$

ACKNOWLEDGMENTS

I thank Prof. Antonio Linero for guiding me through the analytic derivation of the normal ratio distribution. I also thank Dr. Pablo Giuliani for many useful comments and a critical reading of the manuscript. This material is based upon work supported by the U.S. Department of Energy Office of Science, Office of Nuclear Physics under Award DE-FG02-92ER40750.

-
- [1] M. Thiel, C. Sfienti, J. Piekarewicz, C. J. Horowitz, and M. Vanderhaeghen, *J. Phys.* **G46**, 093003 (2019).
 - [2] P. Demorest, T. Pennucci, S. Ransom, M. Roberts, and J. Hessels, *Nature* **467**, 1081 (2010).
 - [3] J. Antoniadis, P. C. Freire, N. Wex, T. M. Tauris, R. S. Lynch, *et al.*, *Science* **340**, 6131 (2013).
 - [4] H. T. Cromartie *et al.*, *Nat. Astron.* **4**, 72 (2019).
 - [5] E. Fonseca *et al.*, (2021), arXiv:2104.00880 [astro-ph.HE].
 - [6] T. E. Riley *et al.*, *Astrophys. J. Lett.* **887**, L21 (2019).
 - [7] M. C. Miller *et al.*, *Astrophys. J. Lett.* **887**, L24 (2019).
 - [8] M. C. Miller *et al.*, (2021), arXiv:2105.06979 [astro-ph.HE].
 - [9] T. E. Riley *et al.*, (2021), arXiv:2105.06980 [astro-ph.HE].
 - [10] G. Raaijmakers, S. K. Greif, K. Hebeler, T. Hinderer, S. Nissanke, A. Schwenk, T. E. Riley, A. L. Watts, J. M. Lattimer, and W. C. G. Ho, (2021), arXiv:2105.06981 [astro-ph.HE].
 - [11] B. P. Abbott *et al.* (Virgo, LIGO Scientific), *Phys. Rev. Lett.* **119**, 161101 (2017).
 - [12] S. Abrahamyan, Z. Ahmed, H. Albatineh, K. Aniol, D. S. Armstrong, *et al.*, *Phys. Rev. Lett.* **108**, 112502 (2012).
 - [13] C. J. Horowitz, Z. Ahmed, C. M. Jen, A. Rakhman, P. A. Souder, *et al.*, *Phys. Rev.* **C85**, 032501 (2012).
 - [14] D. Adhikari *et al.* (PREX), *Phys. Rev. Lett.* **126**, 172502 (2021).
 - [15] A. Tamii *et al.*, *Phys. Rev. Lett.* **107**, 062502 (2011).
 - [16] A. Tamii, P. von Neumann-Cosel, and I. Poltoratska, *Eur. Phys. J.* **A50**, 28 (2014).
 - [17] O. Wieland *et al.*, *Phys. Rev. Lett.* **102**, 092502 (2009).
 - [18] D. Rossi, P. Adrich, F. Aksouh, H. Alvarez-Pol, T. Aumann, *et al.*, *Phys. Rev. Lett.* **111**, 242503 (2013).
 - [19] T. Hashimoto *et al.*, *Phys. Rev.* **C92**, 031305 (2015).
 - [20] J. Birkhan *et al.*, *Phys. Rev. Lett.* **118**, 252501 (2017).
 - [21] A. P. Tonchev *et al.*, *Phys. Lett.* **B773**, 20 (2017).
 - [22] S. Bassauer *et al.*, *Phys. Lett. B* **810**, 135804 (2020).
 - [23] B. A. Brown, *Phys. Rev. Lett.* **85**, 5296 (2000).
 - [24] R. J. Furnstahl, *Nucl. Phys.* **A706**, 85 (2002).
 - [25] M. Centelles, X. Roca-Maza, X. Viñas, and M. Warda, *Phys. Rev. Lett.* **102**, 122502 (2009).
 - [26] X. Roca-Maza, M. Centelles, X. Viñas, and M. Warda, *Phys. Rev. Lett.* **106**, 252501 (2011).
 - [27] W. Satula, R. A. Wyss, and M. Rafalski, *Phys. Rev.* **C74**, 011301 (2006).
 - [28] X. Roca-Maza, M. Centelles, X. Viñas, M. Brenna, G. Colò, *et al.*, *Phys. Rev.* **C88**, 024316 (2013).
 - [29] X. Roca-Maza, X. Viñas, M. Centelles, B. K. Agrawal, G. Colò, N. Paar, J. Piekarewicz, and D. Vretenar, *Phys. Rev.* **C92**, 064304 (2015).
 - [30] J. M. Lattimer and M. Prakash, *Phys. Rept.* **442**, 109 (2007).
 - [31] C. Drischler, R. Furnstahl, J. Melendez, and D. Phillips, *Phys. Rev. Lett.* **125**, 202702 (2020).
 - [32] L.-W. Chen, C. M. Ko, B.-A. Li, and J. Xu, *Phys. Rev.* **C82**, 024321 (2010).
 - [33] A. Steiner and S. Gandolfi, *Phys. Rev. Lett.* **108**, 081102 (2012).
 - [34] J. M. Lattimer, *Ann. Rev. Nucl. Part. Sci.* **62**, 485 (2012).
 - [35] Z. Zhang and L.-W. Chen, *Phys. Lett.* **B726**, 234 (2013).
 - [36] K. Hebeler, J. Lattimer, C. Pethick, and A. Schwenk, *Astrophys. J.* **773**, 11 (2013).
 - [37] S. Gandolfi, J. Carlson, S. Reddy, A. Steiner, and R. Wiringa, *Eur. Phys. J.* **A50**, 10 (2014).
 - [38] G. Hagen *et al.*, *Nature Phys.* **12**, 186 (2016).
 - [39] B. T. Reed, F. J. Fattoyev, C. J. Horowitz, and J. Piekarewicz, *Phys. Rev. Lett.* **126**, 172503 (2021).
 - [40] J. Piekarewicz, *Eur. Phys. J. A* **50**, 25 (2013).
 - [41] J. Yang and J. Piekarewicz, arXiv:1912.11112 [nucl-th].
 - [42] H. Mueller and B. D. Serot, *Nucl. Phys.* **A606**, 508 (1996).
 - [43] C. J. Horowitz and J. Piekarewicz, *Phys. Rev. Lett.* **86**, 5647 (2001).
 - [44] J. D. Walecka, *Annals Phys.* **83**, 491 (1974).
 - [45] B. D. Serot and J. D. Walecka, *Adv. Nucl. Phys.* **16**, 1 (1986).
 - [46] B. D. Serot and J. D. Walecka, *Int. J. Mod. Phys.* **E6**, 515 (1997).
 - [47] W.-C. Chen and J. Piekarewicz, *Phys. Rev.* **C90**, 044305 (2014).
 - [48] A. L. Fetter and J. D. Walecka, “Quantum theory of many particle systems,” (McGraw-Hill, New York, 1971).

- [49] W. H. Dickhoff and D. Van Neck, “Many-body theory exposed,” (World Scientific Publishing Co., 2005).
- [50] M. N. Harakeh and A. van der Woude, “Giant resonances-fundamental high-frequency modes of nuclear excitation,” (Clarendon, Oxford, 2001).
- [51] P.-G. Reinhard and W. Nazarewicz, Phys. Rev. **C81**, 051303(R) (2010).
- [52] J. Piekarewicz, B. Agrawal, G. Colò, W. Nazarewicz, N. Paar, *et al.*, Phys. Rev. **C85**, 041302(R) (2012).
- [53] W.-C. Chen and J. Piekarewicz, Phys. Lett. **B748**, 284 (2015).
- [54] F. J. Fattoyev and J. Piekarewicz, Phys. Rev. Lett. **111**, 162501 (2013).
- [55] P.-G. Reinhard, J. Piekarewicz, W. Nazarewicz, B. Agrawal, N. Paar, *et al.*, Phys.Rev. **C88**, 034325 (2013).
- [56] “CREX: Parity-violating measurement of the weak charge distribution of ^{48}Ca ,” <http://hallaweb.jlab.org/parity/prex/c-rex/c-rex.pdf>.
- [57] M. H. Mahzoon, M. C. Atkinson, R. J. Charity, and W. H. Dickhoff, Phys. Rev. Lett. **119**, 222503 (2017).
- [58] C. D. Pruitt, R. J. Charity, L. G. Sobotka, M. C. Atkinson, and W. H. Dickhoff, Phys. Rev. Lett. **125**, 102501 (2020).
- [59] D. Geesaman *et al.*, “Reaching for the horizon; the 2015 long range plan for nuclear science,” (2015).
- [60] P.-G. Reinhard and W. Nazarewicz, Phys. Rev. **C87**, 014324 (2013).
- [61] J. Piekarewicz, Phys. Rev. **C83**, 034319 (2011).
- [62] W. Płaczek *et al.*, Acta Phys. Polon. B **50**, 1191 (2019).
- [63] W. Płaczek *et al.* (Gamma Factory Working Group), Acta Phys. Polon. Supp. **13**, 645 (2020).
- [64] J. Piekarewicz, (2021), arXiv:2104.11013 [nucl-th].
- [65] N. Paar, D. Vretenar, E. Khan, and G. Colò, Rept. Prog. Phys. **70**, 691 (2007).
- [66] N. Paar, J. Phys. **G37**, 064014 (2010).
- [67] A. Carbone, G. Colò, A. Bracco, L.-G. Cao, P. F. Bortignon, *et al.*, Phys. Rev. **C81**, 041301 (2010).
- [68] D. Savran, T. Aumann, and A. Zilges, Prog. Part. Nucl. Phys. **70**, 210 (2013).
- [69] A. Bracco, E. G. Lanza, and A. Tamii, Prog. Part. Nucl. Phys. **106**, 360 (2019).
- [70] J. Piekarewicz, Phys. Rev. **C73**, 044325 (2006).
- [71] P. Adrich *et al.*, Phys. Rev. Lett **95**, 132501 (2005).
- [72] R. Essick, I. Tews, P. Landry, and A. Schwenk, (2021), arXiv:2102.10074 [nucl-th].
- [73] D. Becker *et al.*, (2018), 10.1140/epja/i2018-12611-6, arXiv:1802.04759 [nucl-ex].
- [74] A. Mann, Nature (London) **579**, 20 (2020).